Polymer Chemistry

ROYAL SOCIETY OF CHEMISTRY

PAPER

View Article Online
View Journal | View Issue

Cite this: *Polym. Chem.*, 2024, **15**, 4637

Functionalization of nano-objects in living anionic polymerization-induced self-assembly and their use for improving thermal properties of epoxy resins

Guicun Guo, Jiali Wu, Jingwei Zhang, Peng Zhou, Ding Shen, Penghan Li and Guowei Wang *

Nano-objects generated *via* a scalable polymerization-induced self-assembly (PISA) process can serve as organic nanofillers, replacing the widely used inorganic nanofillers in composites. In this contribution, polyisoprene (PI)-*b*-polystyrene (PS) (PI-*b*-PS) or PI-*b*-PS/PS nano-objects were prepared *via* a living anionic polymerization-induced self-assembly (LAPISA) process or a derived process of living anionic polymerization-induced cooperative assembly (LAPICA) using nonpolar *n*-heptane as a solvent, which facilitated the control over morphologies and sizes. After the living species in the core region were *in situ* crosslinked by divinylbenzene (DVB) monomers, stabilized PDVB@(PI-*b*-PS) or PDVB@(PI-*b*-PS/PS) nano-objects were generated. After hydroxylated or epoxidized nano-objects were obtained through thiol–ene or epoxidation reactions on the double bonds of the PI stabilizer, the miscibility between the nano-objects and epoxy resin was improved, and the functionalized nano-objects could be introduced into epoxy resin. Differential scanning calorimetry (DSC), thermogravimetric analysis (TGA) and thermomechanical analysis (TMA) results affirmed that the organic nano-objects could improve the thermal properties of the composites, which were obviously superior to commercial inorganic silica nano-objects. In particular, the composites with smaller spherical nano-objects had a higher glass transition temperature (T_g) than those with larger spherical ones or worm-like ones. Transmission electron microscopy (TEM) measurements verified the uniform distribution of organic nano-objects and the formation of sufficiently integrated interfaces between the epoxy resin and nano-objects, thereby improving the thermal properties of the composites.

Received 11th September 2024,
Accepted 22nd October 2024

DOI: 10.1039/d4py01008f

rsc.li/polymers

Introduction

Epoxy resin, after being chemically crosslinked with amines, anhydrides, imidazoles, *etc*., can be widely used in adhesives, coatings, and composites.[1–7] As important thermosetting materials, epoxy resin composites feature excellent corrosion resistance, heat resistance, chemical stability, *etc*.[8] However, the intrinsic tensile strength, glass transition temperature (T_g) and Young's modulus of epoxy resin composites are always lowered due to the introduction of flexible curing agents, such as polyether-amine.[9–11] Thus, high-strength application scenarios are still limited, while being urgently required.[12,13] Generally, the enhancement of epoxy resin composites can be realized by incorporating inorganic nanofillers such as nano-silica,[14,15] alumina,[16,17] glass fibers,[18,19] and so on.[20–24] However, inorganic nanofillers have relatively poor dispersibility in epoxy resin. To optimize the function of the nanofillers, the surface of inorganic nanofillers should be pre-treated or a powerful dispersing device employed to avoid the possible aggregation.[25–27] These processes are troublesome, as well as resulting in low production efficiency. Nevertheless, the inevitable separated interfaces between inorganic nanofillers and epoxy resin have a negative effect on the physicochemical properties of the composites.[28–30] Alternatively, organic nanofillers can be sufficiently mixed and fused with the epoxy resin, and the interfaces can be integrated. Thus, the function of organic nanofillers and the epoxy resin can be maximized, and the properties of the epoxy resin composites can be enhanced. However, organic-nanofiller-enhanced epoxy resin composites are still rarely used. The reason might be the limited availability of nanofillers with scalable production and synergistic effects on the overall properties of epoxy resin composites.[31]

State Key Laboratory of Molecular Engineering of Polymers, Department of Macromolecular Science, Fudan University, Shanghai 200433, China. E-mail: gwwang@fudan.edu.cn

Recently, polymerization-induced self-assembly (PISA) has become an effective technique to prepare nano-objects with diverse morphologies and high solid contents (up to 50 w/w%).[32–51] The preliminary works showed that nano-objects from the PISA process had potential applications in multiple fields.[52–54] For example, the pioneering work by Rieger *et al.* showed that nanofibers with a high T_g could be used as reinforcing fillers for soft acrylic water-based coatings.[55] However, further development of the application of PISA-based nano-objects was still challenging. The reason might be either the difficult synthesis of organic nano-objects with scalable production or the immature theory on the structure–property relationships of organic nano-object-based composites. Among all the controlled/living polymerization mechanisms, living anionic polymerization (LAP) has the characteristics of providing 100% monomer conversion, narrow molecular weight distributions (MWDs), controllable molecular weights (MWs) and monomer sequences, and well-defined structures.[56,57] With these advantages in mind, previously, we have successfully synthesized nano-objects with polyisoprene (PI) as a stabilizer and polystyrene (PS) as the core using a living anionic polymerization-induced self-assembly (LAPISA) process or the derived process of living anionic polymerization-induced cooperative assembly (LAPICA).[48,49] Uniquely, in the LAPISA or LAPICA process, the living species in the core region could be *in situ* crosslinked and the nano-objects could be stabilized. Due to the living and controlled characters of LAP, both the crosslinking position and crosslinking density in the core region could be effectively modulated. Given the controlled crosslinking and stabilization of the nano-objects, the morphologies formed in the LAPISA or LAPICA process could be fixed, which could impart the functions of nano-objects into certain practical applications.

Aiming to explore the application of nano-objects generated in the LAPISA or LAPICA process, herein, nano-objects were selectively modified and introduced into epoxy resin. In detail, PI-*b*-PS or PI-*b*-PS/PS nano-objects were firstly prepared *via* a LAPISA or LAPICA process using styrene (St) and isoprene (Is) as monomers, *n*-heptane as a solvent, *n*-butyllithium (*n*-Bu$^-$Li$^+$) as an initiator, and *N*,*N*,*N*′,*N*′-tetramethylethylenediamine (TMEDA) as a regulator (Scheme 1). The living species in the core region were *in situ* crosslinked with divinylbenzene (DVB) monomers and stabilized PDVB@(PI-*b*-PS) or PDVB@(PI-*b*-PS/PS) nano-objects were generated. Using the efficient thiol–ene or epoxidation reaction, the double bonds on the PI stabilizer were hydroxylated or epoxidized. Subsequently, the functionalized nano-objects were introduced into epoxy resin. Size exclusion chromatography (SEC), proton nuclear magnetic resonance (^{1}H NMR) and dynamic light scattering (DLS) measurements were employed to characterize the compositions and structures of the copolymers and nano-objects. Differential scanning calorimetry (DSC), thermogravimetric analysis (TGA) and thermomechanical analysis (TMA) measurements were used to evaluate the thermal properties of the epoxy resin composites. Furthermore, transmission electron microscopy (TEM) measurements were performed and the possible reason for the improved properties was deduced.

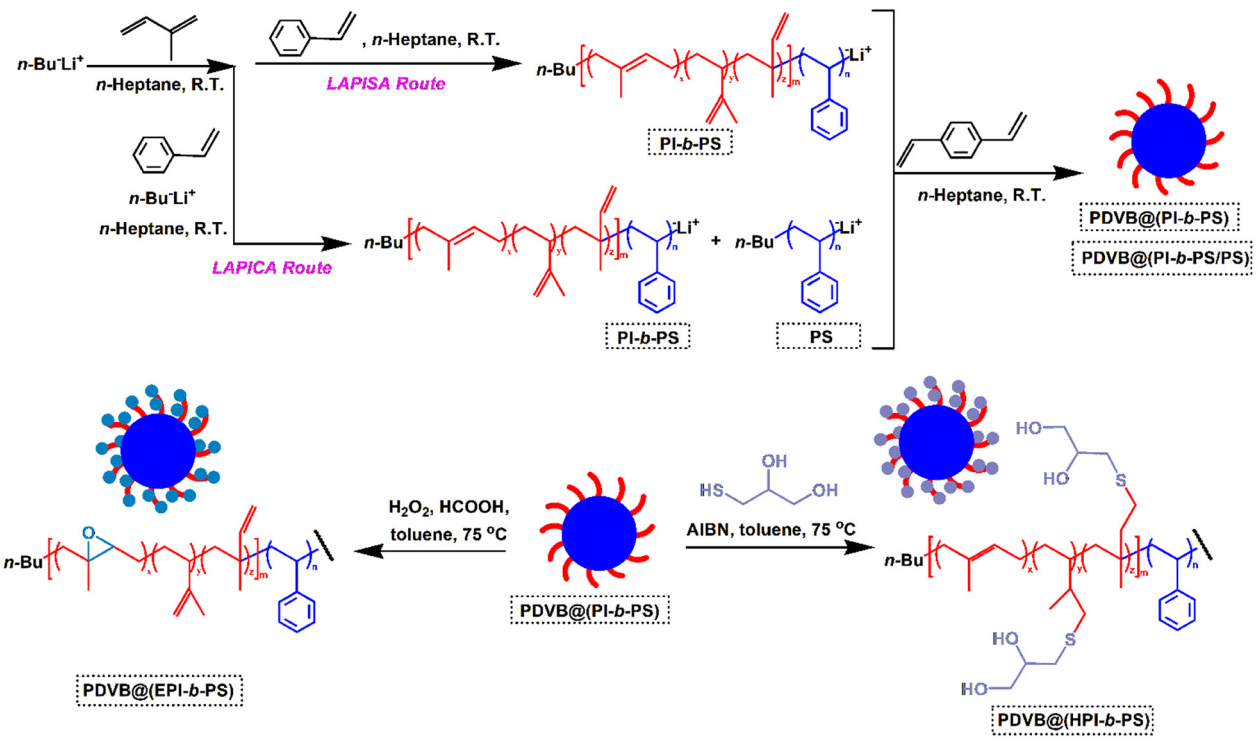

Scheme 1 Illustration of the synthetic route for hydroxylated and epoxidized nano-objects.

Results and discussion

Synthesis and characterization of hydroxylated or epoxidized nano-objects

With reference to our previous works,[48,49] the typical PI-*b*-PS and PI-*b*-PS/PS nano-objects were prepared *via* a LAPISA or LAPICA process using *n*-heptane as a solvent, *n*-Bu$^-$Li$^+$ as an initiator, and TMEDA as a regulator. First, the PI$^-$Li$^+$ macroinitiator was synthesized *via* a homogeneous LAP process of the Is monomer using *n*-Bu$^-$Li$^+$ as an initiator. Subsequently, the St monomer was added and PI-*b*-PS nano-objects were generated in a heterogeneous LAPISA process due to the decreased solubility of the PS core in *n*-heptane. Alternatively, accompanied with the addition of the St monomer, *n*-Bu$^-$Li$^+$ was also supplied and PI-*b*-PS/PS nano-objects were obtained *via* a LAPICA process. Finally, the difunctional DVB monomers (30 wt% relative to St) was added to crosslink the living species in the core region and the nano-objects were stabilized. According to the typical mechanism of PISA,[58–60] after the crosslinking or stabilization, the PDVB formed the innermost core, the PS composed the interlayer and the PI served as the outermost shell. Thus, the nano-objects were labelled as PDVB@(PI-*b*-PS) or PDVB@(PI-*b*-PS/PS). Obviously, in the LAPISA process, the nano-objects were generated from a PI-*b*-PS diblock copolymer. Alternatively, in the LAPICA process, the nano-objects were generated from a PI-*b*-PS diblock copolymer and PS homopolymer, which were cooperatively self-assembled. Uniquely, it should be mentioned that the P(S_{317}-*co*-DVB_{90})@PI_{243} nano-objects were prepared by simultaneous addition of St and DVB monomers, and $PDVB_{129}$@PI_{239} nano-objects were prepared without addition of St monomers. Comprehensively using the LAPISA or LAPICA process,[48,49] nano-objects with different sizes and morphologies were synthesized by varying the degree of polymerization of PI (DP_{PI}) and PS (DP_{PS}), as well as the addition mode of the St monomer and *n*-Bu$^-$Li$^+$ initiator (Table 1). The successful synthesis of the nano-objects facilitated the applications in this work.

As per the SEC traces shown in Fig. 1(A and B), the PI macroinitiator precursor, PI-*b*-PS diblock copolymer and PS homopolymer were obtained with controlled MWs and narrow M_w/M_ns. From the ^{1}H NMR spectrum for the stabilized $PDVB_{25}$@(PI_{82}-*b*-PS_{105}) nano-objects, shown in Fig. 2(A), the characteristic resonance signal for phenyl protons (–$C_6\boldsymbol{H}_5$) on the PS block was assigned between 6.27–6.84 ppm. On the PI block, the resonance signal for the alkene proton (CH_2=C$\boldsymbol{H}$–) on the 3,4-addition Is unit was assigned at 5.76 ppm, and the alkene protons (–C(CH_3)=C$\boldsymbol{H}$–, C$\boldsymbol{H}_2$=C(CH_3)–, C$\boldsymbol{H}_2$=CH–) on the 1,4-addition, 1,2-addition, and 3,4-addition Is units were assigned between 4.47–5.34 ppm. According to the ^{1}H NMR spectrum in Fig. 2(A), the content of 1,4-addition, 1,2-addition, and 3,4-addition Is units in $PDVB_{25}$@(PI_{82}-*b*-PS_{105}) could be calculated as 22.8%, 14.3% and 62.9%, respectively. Similarly, according to the ^{1}H NMR spectrum in Fig. 2(B), the content of 1,4-addition, 1,2-addition, and 3,4-addition Is units in $PDVB_{25}$@(PI_{76}-*b*-PS_{103}) could be calculated as 64.7%, 0%, and 35.3%, respectively. It should be mentioned that the content of different addition units could be adjusted by modulating the molar ratio of the TMEDA mediator to *n*-Bu$^-$Li$^+$ initiator. From the DLS curves shown in Fig. 3(A–C), it could be found that the nano-objects were stable in THF, and stabilized nano-objects with different sizes were actually achieved when modulating the DP_{PI} and DP_{PS}, as well as the polymerization technology. Comparatively, the unstabilized PI_{76}-*b*-PS_{92} diblock copolymer showed a size of around 2.0 nm in the DLS curve, indicating completely dissolved macromolecules, as THF was a good solvent for both PI and PS blocks.

Due to the relatively low polarity of the PI block, the copolymers or nano-objects had low miscibility or compatibility with the employed epoxy resin of UVR-6110. Thus, a suspension was always formed when directly adding the nano-objects into the epoxy resin. Aiming to improve the

Table 1 The formulation and characterization of the nano-objects and their precursors[a]

		PI		PI-*b*-PS or PI-*b*-PS/PS					
Samples[b]	Targeted $M_{n,PS}/M_{n,PI}$	$M_{n,PI}$[c]/ g mol^{-1}	M_w/M_n[c]	$M_{n,PI\text{-}b\text{-}PS}$[c]/ g mol^{-1}	M_w/M_n[c]	$M_{n,PS}$[c]/ g mol^{-1}	M_w/M_n[c]	Morphologies[d]	Sizes[e] (nm)
PI_{76}-*b*-PS_{92}	2/1	5300	1.05	14 800	1.08				
$PDVB_{26}$@(PI_{85}-*b*-PS_{75}/PS_{38})	2/1	5800	1.09	13 600	1.06	3900	1.06	Sphere	680
$PDVB_{25}$@(PI_{82}-*b*-PS_{105})	2/1	5600	1.09	16 500	1.06			Sphere	43
$PDVB_{60}$@(PI_{86}-*b*-PS_{228})	4/1	5800	1.06	29 500	1.06			Worm	450
$PDVB_{129}$@PI_{239}	1/1	16 300	1.06					Sphere	58
P(S_{317}-*co*-DVB_{90})@PI_{243}	2/1	16 600	1.05					Sphere	66
$PDVB_{82}$@(PI_{252}-*b*-PS_{313})	2/1	17 200	1.13	49 700	1.09			Sphere	50
$PDVB_{84}$@(PI_{228}-*b*-PS_{203}/PS_{169})	2/1	15 600	1.14	36 600	1.06	17 600	1.07	Sphere	530
$PDVB_{25}$@(PI_{76}-*b*-PS_{103})	2/1	5100	1.06	15 800	1.04			Sphere	41
$PDVB_{73}$@(PI_{202}-*b*-PS_{278})	2/1	13 700	1.08	42 600	1.06			Sphere	50

[a] The solid content was set as 20% w/w. [b] The subscripts represented the DP of each block, which could be calculated using the $M_{n,PI}$, targeted $M_{n,PS}/M_{n,PI}$ and the fed DVB (30 wt% relative to St). [c] The M_n and M_w/M_n were obtained *via* SEC measurements using THF as the eluent and PS as the standard. [d] The morphologies of the nano-objects were monitored *via* TEM measurements. [e] The sizes of the nano-objects were obtained *via* DLS measurements.

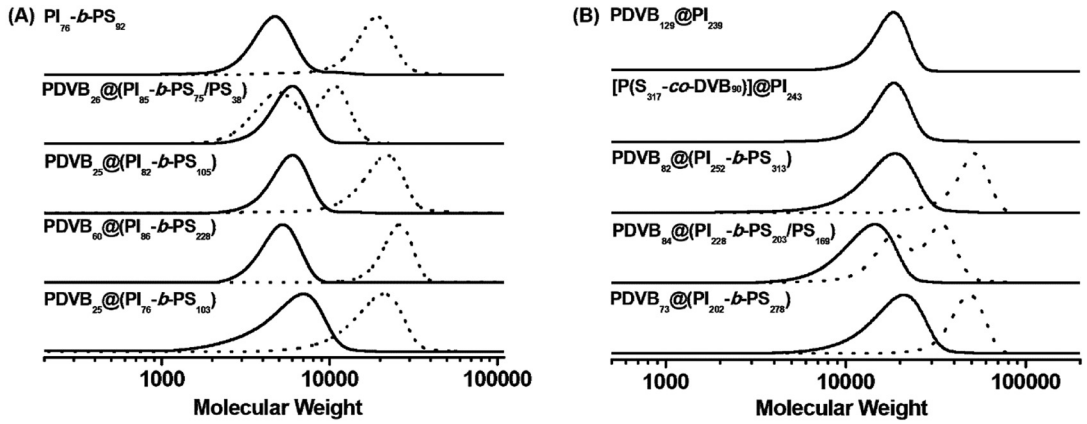

Fig. 1 SEC traces of the PI macroinitiator (solid line), PI-*b*-PS diblock copolymer and PS homopolymer (dotted line) targeting (A) nano-objects with relatively short PI blocks (DP between 76 and 92), and (B) nano-objects with relatively long PI blocks (DP between 202 and 252) (using THF as the eluent and PS as the standard).

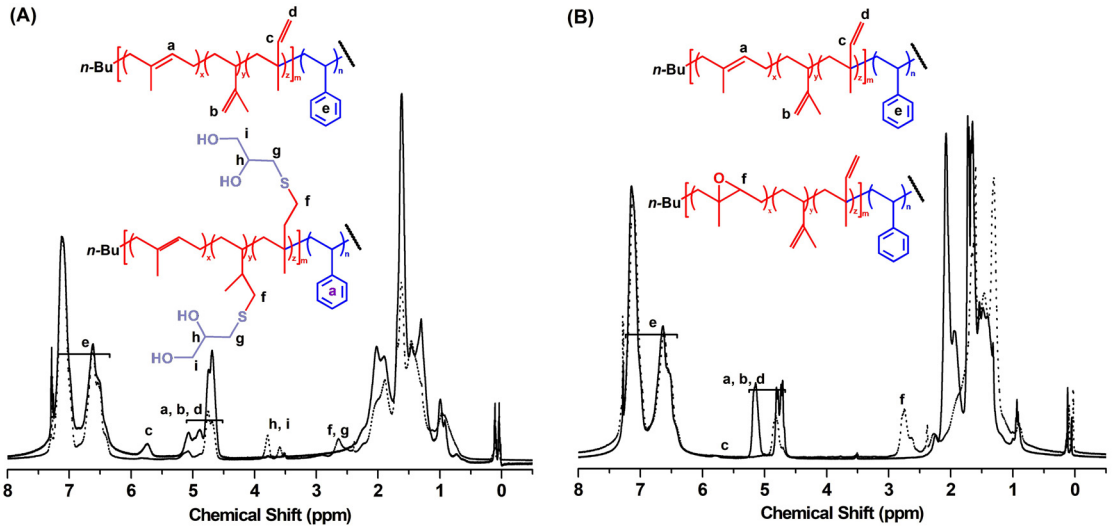

Fig. 2 ^{1}H NMR spectra for (A) $PDVB_{25}$@(PI_{82}-*b*-PS_{105}) (solid line) and $PDVB_{25}$@(HPI_{82}-*b*-PS_{105}) (dotted line), and (B) $PDVB_{25}$@(PI_{76}-*b*-PS_{103}) (solid line) and $PDVB_{25}$@(EPI_{76}-*b*-PS_{103}) (dotted line) (using $CDCl_3$ as the solvent).

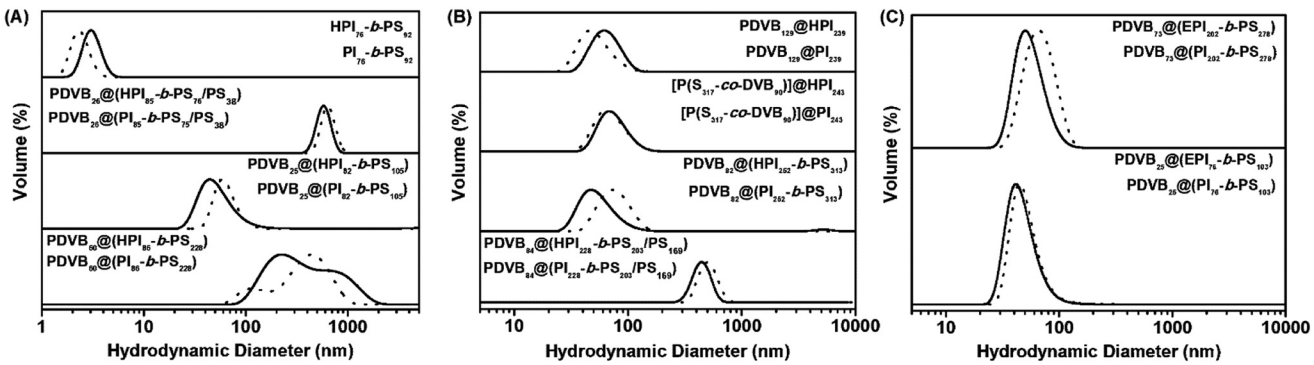

Fig. 3 DLS of (A) original (solid line) and hydroxylated (dotted line) diblock copolymer or nano-objects with relatively short PI block (DP between 76 and 92), (B) original (solid line) and hydroxylated (dotted line) nano-objects with relatively long PI block (DP between 202 and 252), and (C) original (solid line) and epoxidized (dotted line) nano-objects (using THF as the solvent).

miscibility or compatibility, the PI-*b*-PS diblock copolymer, PDVB@(PI-*b*-PS) or PDVB@(PI-*b*-PS/PS) nano-objects were purified and recovered from methanol, and hydroxyl and epoxy groups were introduced onto the PI block *via* thiol–ene or epoxidation reactions using THF and/or toluene as the solvent. It should be mentioned that the adoption of THF and/or toluene was to sufficiently swell the nano-objects and solubilize the outermost PI, as well as to increase the solubility of the polar 3-mercaptopropane-1,2-diol agent or hydrogen peroxide/formic acid (H_2O_2/HCOOH) agents, which facilitated the hydroxylation and epoxidation reaction on the double bond of the PI block. As per the ^{1}H NMR spectrum shown in Fig. 2(A), after the thiol–ene reaction with 3-mercaptopropane-1,2-diol, the characteristic resonance signal at 5.76 ppm attributed to the alkene proton (CH_2═C***H***–) on the 3,4-addition Is unit completely disappeared. The resonance signal attributed to alkene protons (–C(CH_3)═C***H***–, C***H***$_2$═C(CH_3)–, C***H***$_2$═CH–) between 4.47–5.34 ppm was also weakened. Meanwhile, the resonance signal attributed to protons (HOC***H***$_2$C***H***(OH)–) at 3.45–3.90 ppm and protons (–C***H***$_2$SC***H***$_2$–) at 2.42–2.83 ppm could be clearly discriminated. After the epoxidation reaction in the presence of H_2O_2/HCOOH, the resonance signal attributed to the alkene protons (–C(CH_3)═C***H***–) on the 1,4-addition Is units between 4.56–5.26 ppm was significantly reduced (Fig. 2(B)). Meanwhile, a resonance signal between 2.50–2.98 ppm attributed to the epoxy proton (–C(CH_3)OC***H***–) was observed. Based on the ^{1}H NMR spectra, the degree of hydroxylation on PDVB$_{25}$@(HPI$_{82}$-*b*-PS$_{105}$) was calculated as 14.8%, and the degree of epoxidation on PDVB$_{25}$@(EPI$_{76}$-*b*-PS$_{103}$) was calculated as 64.7%. The degrees of functionalization were rather close to the respective contents of 1,2-addition or 1,4-addition Is units on the nano-objects. Thus, the ^{1}H NMR results confirmed that the thiol–ene reaction predominantly happened on the 1,4-addition Is units, while the epoxidation preferred to occur on the 1,4-addition Is units, which was actually consistent with our previous works[61,62] and the literatures.[63,64] The functionalized nano-objects were further characterized *via* DLS measurements using THF as the solvent, which showed close sizes to those before the modification (Fig. 3(A–C)). The consistent sizes between the original and functionalized nano-objects further confirmed the successful stabilization, and additionally, no side reactions happened on the PI block during the modification process.

As shown in Fig. 4, the original PDVB$_{25}$@(PI$_{82}$-*b*-PS$_{105}$) had poor miscibility with the epoxy resin UVR-6110 and was completely suspended on the upper layer. After the hydroxylation reaction, the PDVB$_{25}$@(HPI$_{82}$-*b*-PS$_{105}$) and PDVB$_{26}$@(HPI$_{85}$-*b*-PS$_{75}$/PS$_{38}$), with different sizes, could be effectively dispersed into the epoxy resin, and a clear homogeneous solution was achieved. Uniquely, the dispersibility of the organic nano-objects was somewhat superior to that of inorganic SiO_2-1# and SiO_2-2# nano-objects. The improved miscibility between the nano-objects and epoxy resin greatly facilitated the following application as additives in epoxy resin composites.

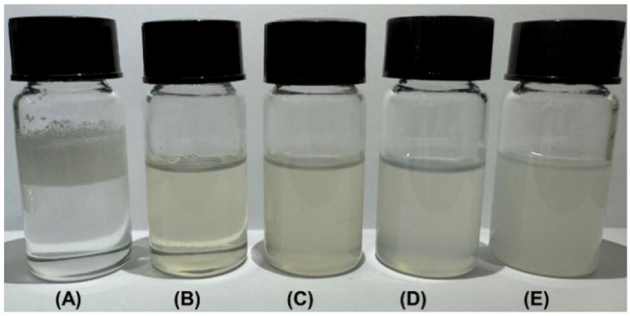

Fig. 4 Pictures of (A) PDVB$_{25}$@(PI$_{82}$-*b*-PS$_{105}$), (B) PDVB$_{25}$@(HPI$_{82}$-*b*-PS$_{105}$), (C) PDVB$_{26}$@(HPI$_{85}$-*b*-PS$_{75}$/PS$_{38}$), (D) SiO_2-1#, and (E) SiO_2-2# dispersions in epoxy resin UVR-6110 at room temperature (25 °C).

Thermal properties of epoxy resin composites improved with nano-objects

Based on the improved miscibility or compatibility of the nano-objects with epoxy resin UVR-6110, the nano-objects were introduced into the epoxy resin. For comparison, the functionalized PI$_{76}$-*b*-PS$_{92}$ diblock copolymer, and inorganic SiO_2-1# and SiO_2-2# were also introduced into the epoxy resin.

As shown in Fig. 5, DSC measurements of the PI$_{76}$-*b*-PS$_{92}$ diblock copolymer and nano-objects before and after functionalization were firstly performed and compared. For the PDVB$_{26}$@(PI$_{85}$-*b*-PS$_{75}$/PS$_{38}$), PDVB$_{25}$@(PI$_{82}$-*b*-PS$_{105}$), and PDVB$_{60}$@(PI$_{86}$-*b*-PS$_{228}$) nano-objects, the T_gs attributed to the crosslinked core were detected at 101.8 °C, 113.8 °C, and 103.4 °C, respectively (Fig. 5(A)). For the PI$_{76}$-*b*-PS$_{92}$ diblock copolymer, a relatively low T_g attributed to the PS block was detected at 81.7 °C. However, in all cases, no T_g attributed to the PI block could be discriminated due to the relatively low DP$_{PI}$s (between 76 and 92). Meanwhile, for the PDVB$_{82}$@(PI$_{252}$-*b*-PS$_{313}$) and PDVB$_{84}$@(PI$_{228}$-*b*-PS$_{203}$/PS$_{169}$) nano-objects with relatively high DP$_{PI}$s (between 202 and 252), the T_gs attributed to the PI block could be detected around 10.7 °C and 11.8 °C, and the T_gs attributed to the crosslinked core were detected at 103.2 °C and 109.1 °C, respectively (Fig. 5(B)). For the PDVB$_{129}$@PI$_{239}$ and P(S$_{317}$-*co*-DVB$_{90}$)@PI$_{243}$ nano-objects, the T_gs attributed to the PI block could be detected around 18.0 °C and 8.7 °C, respectively. However, due to the high crosslinking of the core region, the T_gs for the crosslinked core could not be detected. Furthermore, after the hydroxylation of the nano-objects, the T_gs for the crosslinked core of PDVB$_{82}$@(HPI$_{252}$-*b*-PS$_{313}$) and PDVB$_{84}$@(HPI$_{228}$-*b*-PS$_{203}$/PS$_{169}$) were detected at 95.9 °C and 100.0 °C (Fig. 5(C)), respectively. However, no signal attributed to HPI$_{252}$ or HPI$_{228}$ could be discriminated. The absence of T_gs for HPI$_{252}$ or HPI$_{228}$ might attributed to the introduction of hydroxyl groups onto the PI block. Correspondingly, this result confirmed that the hydroxylation reaction was successfully performed. Comparing all the DSC results in Fig. 5(A–C), it could be discerned that the sizes (from 41 nm to 680 nm) and morphologies (spheres or worms) of the stabilized nano-objects (Table 1) had less effect on the evolution of the T_gs of the cores or stabilizers. Meanwhile, the

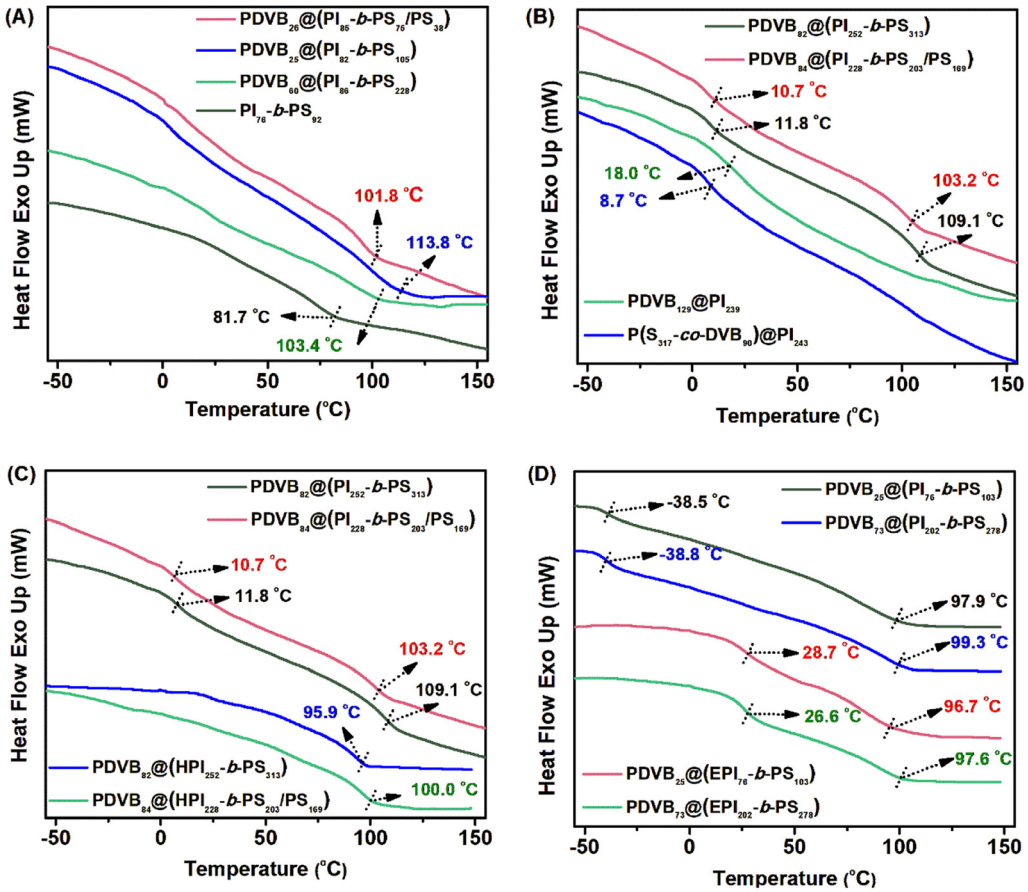

Fig. 5 DSC curves (derived from the second heating run from −65 °C to 150 °C at a heating rate of 10 °C min^{-1} under a nitrogen atmosphere) for (A) the original diblock copolymer or nano-objects with relatively short PI blocks (DP between 76 and 92), (B) the original nano-objects with relatively long PI blocks (DP between 202 and 252), (C) the original $PDVB_{82}$@(PI_{252}-*b*-PS_{313}) and $PDVB_{84}$@(PI_{228}-*b*-PS_{203}/PS_{169}), hydroxylated $PDVB_{82}$@(HPI_{252}-*b*-PS_{313}) and $PDVB_{84}$@(HPI_{228}-*b*-PS_{203}/PS_{169}) nano-objects, and (D) the original $PDVB_{26}$@(PI_{78}-*b*-PS_{101}) and $PDVB_{73}$@(PI_{202}-*b*-PS_{278}), epoxidized $PDVB_{26}$@(EPI_{78}-*b*-PS_{101}) and $PDVB_{73}$@(EPI_{202}-*b*-PS_{278}) nano-objects.

stabilization made a significant contribution to the T_gs of the crosslinked core in comparison with the T_g of the PS block in PI_{76}-*b*-PS_{92}, and the T_gs of the PI block were seriously affected by the DP_{PI}.

For $PDVB_{25}$@(PI_{76}-*b*-PS_{103}) and $PDVB_{73}$@(PI_{202}-*b*-PS_{278}), the T_gs for the PI block were observed at −38.5 °C and −38.8 °C, and the T_gs for the crosslinked core were discriminated at 97.9 °C and 99.3 °C, respectively (Fig. 5(D)). After the epoxidation of the nano-objects, the T_gs for the crosslinked core were observed at 96.7 °C and 97.6 °C, respectively. Meanwhile, the T_gs for the EPI block were observed at 28.7 °C and 26.6 °C, respectively, which were obviously higher than those for the PI blocks before the epoxidation reaction. The reason could be the transformation of the 1,4-addition Is units into epoxy groups, which significantly reduced the softness of the PI block.

Subsequently, the functionalized nano-objects were blended with the epoxy resin UVR-6110 and the thermal properties of the cured epoxy resin composites were investigated *via* DSC measurements. As shown in Fig. 6(A), the T_g of the epoxy resin composites without any additives was 176.6 °C. When the amount of spherical $PDVB_{25}$@(HPI_{82}-*b*-PS_{105}) nano-objects was varied from 4.5 wt% to 15.0 wt%, the T_gs of the epoxy resin composites increased in a regular manner. Meanwhile, the T_gs of the epoxy resin composites were also improved when the amount of spherical $PDVB_{26}$@(HPI_{85}-*b*-PS_{75}/PS_{38}) nano-objects was changed from 4.5 wt% to 9.0 wt%. However, the further addition of $PDVB_{26}$@(HPI_{85}-*b*-PS_{75}/PS_{38}) nano-objects to 15.0 wt% led to a decrease in the T_g. The reason could be the aggregation of the spherical nano-objects at relatively high concentration and with large sizes. Similarly, the addition of 4.5 wt% to 9.0 wt% worm-like $PDVB_{60}$@(HPI_{86}-*b*-PS_{228}) nano-objects contributed to increased T_gs of the epoxy resin composites. However, when the amount of $PDVB_{60}$@(HPI_{86}-*b*-PS_{228}) was increased to 15.0 wt%, the nano-objects could not be efficiently dispersed into the epoxy resin. The reason could be explained as the serious entanglement of the worm-like nano-objects at relatively high concentration. Herein, the sizes and morphologies exhibited a significant effect on the T_gs of the cured epoxy resin composites. The composites with smaller spherical $PDVB_{25}$@(HPI_{82}-*b*-PS_{105}) nano-objects (43 nm) showed higher T_gs than those with the

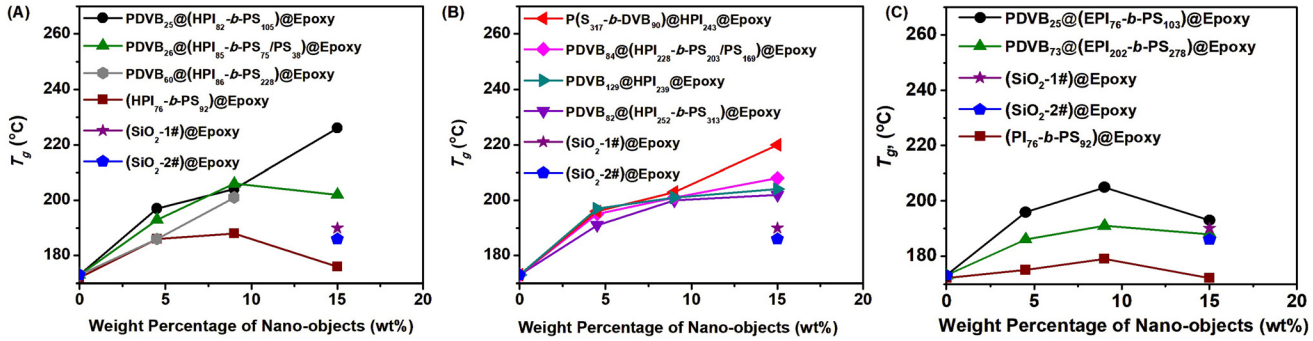

Fig. 6 Evolution of T_gs (derived from the second heating run from 25 °C to 250 °C at a heating rate of 10 °C min^{-1} under a nitrogen atmosphere) for cured epoxy resin composites improved with (A) hydroxylated diblock copolymer or nano-objects with relatively short PI blocks (DP between 76 and 92), (B) hydroxylated nano-objects with relatively long PI blocks (DP between 202 and 252), and (C) epoxidized nano-objects, and comparison of the T_gs with those improved with SiO_2-1# and SiO_2-2# nano-objects.

larger spherical PDVB$_{26}$@(HPI$_{85}$-*b*-PS$_{75}$/PS$_{38}$) nano-objects (680 nm) or worm-like PDVB$_{60}$@(HPI$_{86}$-*b*-PS$_{228}$) nano-objects (450 nm). Comparatively, the hydroxylated PI$_{76}$-*b*-PS$_{92}$ diblock copolymer showed a reduced contribution to the T_g of the composites with addition from 4.5 wt% to 15.0 wt% (Fig. 6(A)). Obviously, the stabilization of the nano-objects was essential for the additives. Meanwhile, 15.0 wt% of inorganic SiO_2-1# and SiO_2-2# nano-objects were also introduced into the epoxy resin and used for comparison. From Fig. 6(A), it could be found that the improvements of T_g with 15 w/w% inorganic SiO_2-1# and SiO_2-2# were less than those with the stabilized organic nano-objects.

In the above composites, the DP$_{PI}$s were between 76 and 92. The relatively short PI blocks might limit the incorporation of the nano-objects within the epoxy resin matrix. Aiming to improve the miscibility, the nano-objects with higher DP$_{PI}$s (between 202 and 252) were also introduced into the epoxy resin and investigated. As shown in Fig. 6(B), the epoxy resin composites containing PDVB$_{82}$@(HPI$_{252}$-*b*-PS$_{313}$), PDVB$_{84}$@(HPI$_{228}$-*b*-PS$_{203}$/PS$_{169}$), PDVB$_{129}$@HPI$_{239}$, and P(S$_{317}$-*co*-DVB$_{90}$)@HPI$_{243}$ nano-objects contributed to increased T_gs with the addition between 4.5 wt% and 15.0 wt%. Unlike the composites in the above section, at the addition of 15.0 wt%, all the nano-objects could increase the T_g of the epoxy resin composites regardless of the sizes. The reason could be the relatively long HPI block, which further increased the miscibility between the nano-objects and the epoxy resin. That was, at relatively high percentages, the nano-objects could be effectively dispersed in the composites and improvement in the T_g could be realized. Comprehensively comparing the epoxy resin composites containing PDVB$_{82}$@(HPI$_{252}$-*b*-PS$_{313}$) and PDVB$_{84}$@(HPI$_{228}$-*b*-PS$_{203}$/PS$_{169}$) with those containing PDVB$_{129}$@HPI$_{239}$ and P(S$_{317}$-*co*-DVB$_{90}$)@HPI$_{243}$, it should be noted that the topologies of the crosslinked core had less influence on T_gs. Compared with the epoxy resin composites containing the HPI$_{76}$-*b*-PS$_{92}$ diblock copolymer, again, it could be concluded that the stabilization of the nano-objects was essential for the additives. Additionally, with DP$_{PI}$s between 202 and 252, the T_gs of the epoxy resin composites with stabilized organic nano-objects were also higher than those with 15 w/w% of inorganic SiO_2-1# and SiO_2-2#.

As shown in Fig. 6(C), the improvement in the T_gs of epoxy resin composites with epoxidized nano-objects was also investigated. In all cases, the epoxidized PDVB$_{25}$@(EPI$_{76}$-*b*-PS$_{103}$) and PDVB$_{73}$@(EPI$_{202}$-*b*-PS$_{278}$) nano-objects contributed to improved T_gs in the epoxy resin composites. The addition of 9.0 wt% PDVB$_{25}$@(EPI$_{76}$-*b*-PS$_{103}$) and PDVB$_{73}$@(EPI$_{202}$-*b*-PS$_{278}$) nano-objects resulted in the highest T_gs. Thus, the epoxidized nano-objects could be employed as alternative additives to modify the epoxy resin.

Furthermore, TGA measurements were performed and analysed. As demonstrated in Fig. 7(A), the TGA curves showed that the thermal decomposition temperatures of PDVB$_{25}$@(PI$_{82}$-*b*-PS$_{105}$) and PDVB$_{26}$@(PI$_{85}$-*b*-PS$_{75}$/PS$_{38}$) nano-objects were higher than that for the PI$_{76}$-*b*-PS$_{92}$ diblock copolymer, and further higher than that for cured pure epoxy resin. After the curing of the epoxy resin composites containing 15.0 wt% nano-objects, the TGA curves showed distinct thermal decomposition behaviours. From Fig. 7(B), it could be discerned that the epoxy resin composites containing 15.0 wt% PDVB$_{25}$@(PI$_{82}$-*b*-PS$_{105}$) or PDVB$_{26}$@(PI$_{85}$-*b*-PS$_{75}$/PS$_{38}$) nano-objects start to decompose at 310 °C. However, the epoxy resin composites containing 15.0 wt% PI$_{76}$-*b*-PS$_{92}$ diblock copolymer, SiO_2-1# or SiO_2-2# nano-objects had a similar start temperature of 250 °C. Above 450 °C, the PDVB$_{25}$@(PI$_{82}$-*b*-PS$_{105}$)- or PDVB$_{26}$@(PI$_{85}$-*b*-PS$_{75}$/PS$_{38}$)-based composites had a higher content of residue than the PI$_{76}$-*b*-PS$_{92}$-based composite, although these composites had the same amounts of additives. The TGA results showed that the composites with stabilized nano-objects had enhanced resistance to thermal decomposition. That was, the stabilized nano-objects improved the T_gs as well the thermal stability of the composites. Thus, the improvement in the T_gs and thermal stability of the composites by the nano-objects was relevant and consistent.

Besides the DSC and TGA analyses on the epoxy resin composites, the dimensional stability, as an important factor for epoxy resin composites, was also characterized *via* TMA

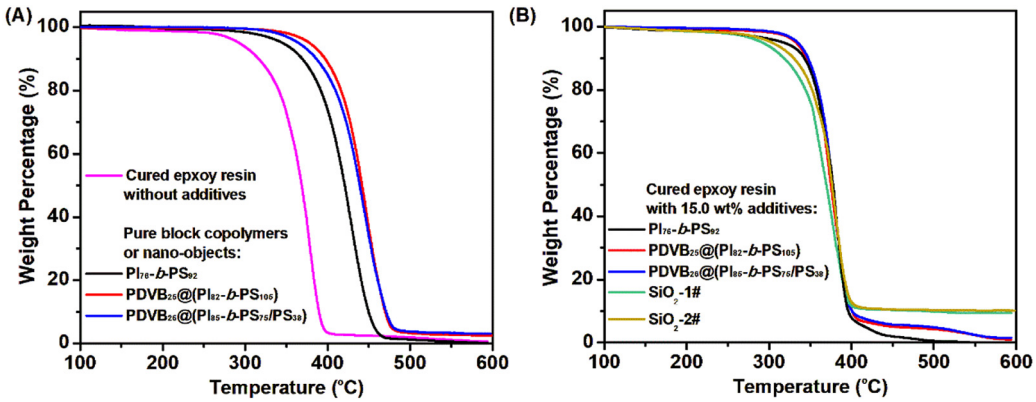

Fig. 7 TGA curves (heating from 50 °C to 600 °C at a heating rate of 10 °C min^{-1} under a nitrogen atmosphere) for (A) cured epoxy resin without additives, pure PI_{76}-*b*-PS_{92} diblock copolymer, pure $PDVB_{25}$@(PI_{82}-*b*-PS_{105}) and pure $PDVB_{26}$@(PI_{85}-*b*-PS_{75}/PS_{38}) nano-objects, and (B) cured epoxy resin with 15.0 wt% additives of PI_{76}-*b*-PS_{92} diblock copolymer, $PDVB_{25}$@(PI_{82}-*b*-PS_{105}), $PDVB_{26}$@(PI_{85}-*b*-PS_{75}/PS_{38}), SiO_2-1# or SiO_2-2# nano-objects.

measurements. From Fig. 8, it could be observed that the coefficients of thermal expansion (CTEs) of all the epoxy resin composites were similar to that for pure epoxy resin. That is, the introduction of nano-objects has no deteriorative effect on the dimensional stability of the composites and could be applied as an efficient strategy to modify the epoxy resin.

Thus, all the thermal analyses confirmed that the stabilized nano-objects contributed a positive effect on the thermal properties of the epoxy resin composites. The reason could be proposed as the following. The hydroxyl or epoxy groups on the periphery of the nano-objects might take part in the crosslinking reaction with the epoxy resin to form a dense network. Meanwhile, the crosslinked core region of the nano-objects themselves was also a dense network. Additionally, due to the excellent miscibility between the nano-objects and epoxy resin, the nano-objects could be homogeneously dispersed. Thus, the nano-objects and epoxy resin were sufficiently mixed, and a dense network in the cured epoxy resin could be formed. Correspondingly, the improvement in the T_gs of the epoxy resin composites was realized.

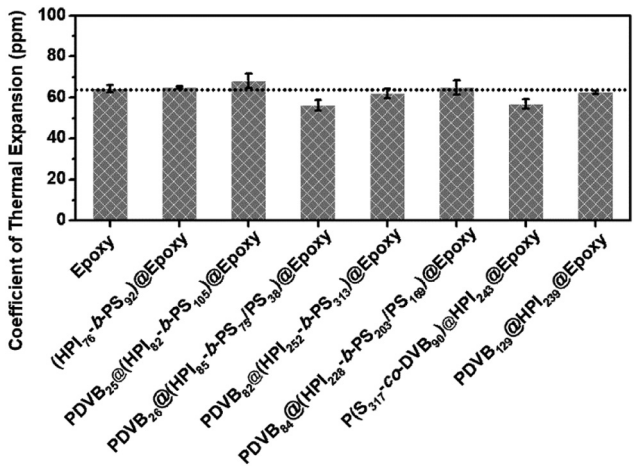

Fig. 8 Evolution of the CTE for the cured epoxy resin composites containing 15.0 wt% diblock copolymer or nano-objects.

Finally, aiming to monitor the distribution of the nano-objects in the epoxy resin composites, TEM measurements were performed and analysed. As shown in Fig. 9, the stabilized original or hydroxylated nano-objects with spherical (Fig. 9(a, b, d and e)) and worm-like (Fig. 9(g and h)) morphologies could be effectively dispersed in THF, and good maintenance of the sizes and morphologies in THF further revealed that the nano-objects were stable. Meanwhile, the TEM results were rather consistent with those from the DLS measurements (Fig. 9(l)). After the introduction of the nano-objects into the cured epoxy resin, the spherical (Fig. 9(c and f)) or worm-like (Fig. 9(i)) morphologies could still be discerned. Meanwhile, it was found that the nano-objects could be uniformly dispersed in the epoxy resin composites. Consistent with the above analyses of the T_gs of the composites, the homogeneity of larger spherical nano-objects was inferior to that of smaller spherical ones. In particular, the serious entanglement of the worm-like structures resulted in the poor dispersion of the nano-objects in epoxy resin. Thus, the conclusion that the nano-objects with relatively small sizes and spherical morphologies contributed to the best thermal properties was supported by the TEM results. Similarly, the reference inorganic SiO_2-1# and SiO_2-2# nano-objects could be also uniformly dispersed into the epoxy resin composites (Fig. 9(j and k)). However, with close weight percentages, the numbers of inorganic silica nano-objects were less than those of the organic nano-objects. Thus, the improvement of the thermal properties of epoxy resin composites with inorganic SiO_2-1# and SiO_2-2# nano-objects was restricted. Also, it could be observed that the organic nano-objects could be sufficiently blended with the epoxy resin and the interfaces were significantly integrated. However, the inorganic SiO_2-1# and SiO_2-2# nano-objects had clear interfaces with the epoxy resin matrix.

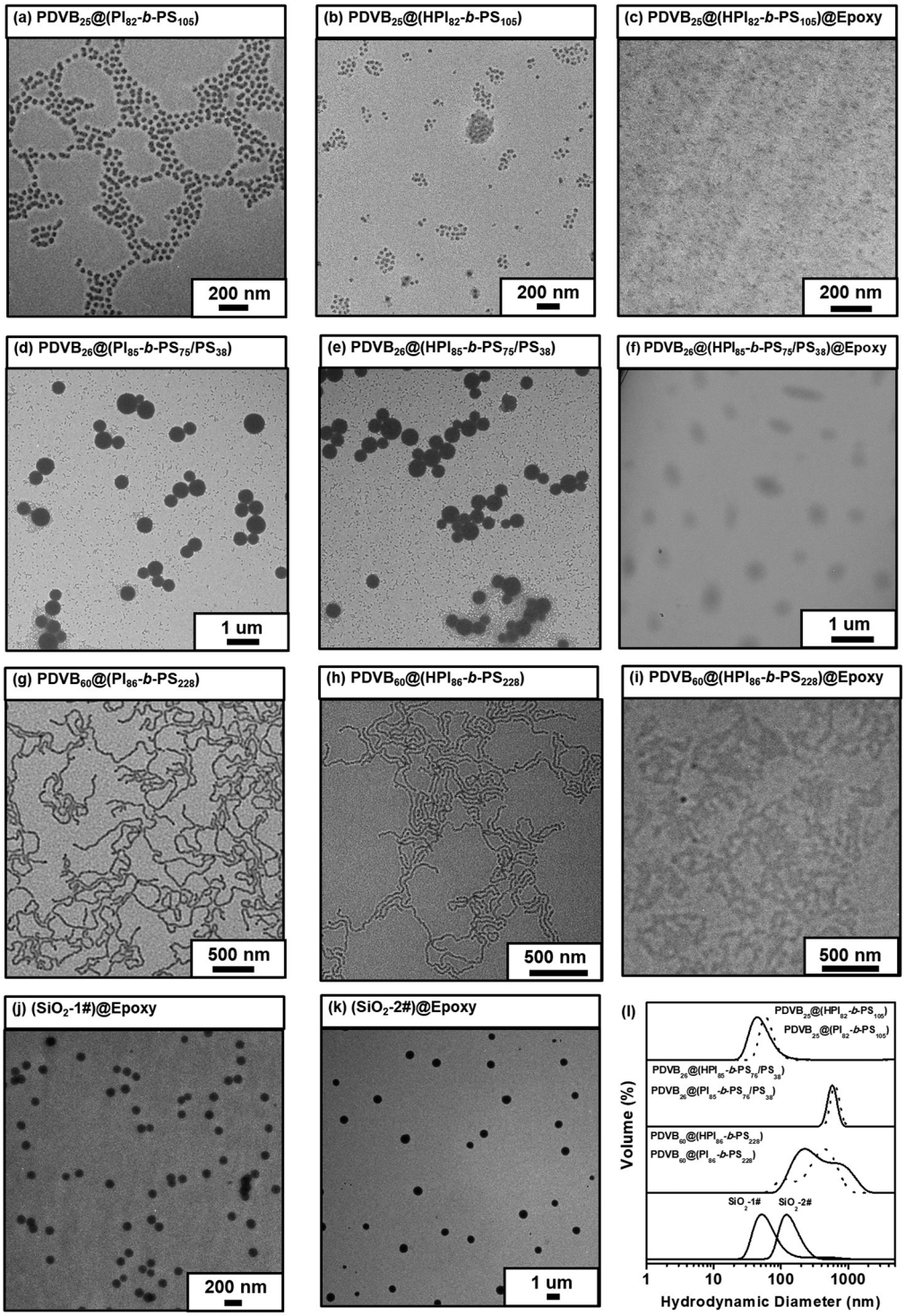

Fig. 9 TEM images of the original nano-objects (a, d, g) and hydroxylated nano-objects (b, e, h) in THF, hydroxylated nano-objects (c, f, i) and SiO_2-1# and SiO_2-2# nano-objects (j, k) in cured epoxy resin composites, and the corresponding DLS results of the original (solid line) and hydroxylated (dotted line) nano-objects in THF (l). The amounts of the PDVB$_{25}$@(HPI$_{82}$-*b*-PS$_{105}$), PDVB$_{26}$@(HPI$_{85}$-*b*-PS$_{75}$/PS$_{38}$) and PDVB$_{60}$@(HPI$_{86}$-*b*-PS$_{228}$) nano-objects were 15.0 wt%, 15.0 wt%, and 9.0 wt%, respectively.

Occasionally, there were some agglomerations of inorganic SiO_2-1# and SiO_2-2# nano-objects. Thus, the TEM measurements provided consistent results with those from the DSC and TGA analyses, which comprehensively confirmed that the stabilized organic nano-objects could be used as novel and efficient nanofillers for epoxy resin composites.

Experimental

Materials

Isoprene (Is, 99.0%, TCI), styrene (St, 99%, Adamas) and *N*,*N*,*N*′,*N*′-tetramethylethylenediamine (TMEDA, 99%, Adamas) were dried over CaH_2, distilled and stored in a refrigerator at −5 °C. *n*-Heptane (99%, Sinopharm Chemical Reagent Co. (SCR)) was dried over CaH_2 and distilled prior to use. *n*-Butyllithium (*n*-Bu$^-$Li$^+$, 1.6 M in hexane, Adamas), 3-mercaptopropane-1,2-diol (98%, TCI), 2,2-azobis(2-methylpropionitrile) (AIBN, 98%, Adamas), 3,4-epoxycyclohexylmethyl-3′,4′-epoxycyclohexanecarboxylate (UVR-6110, Jiangsu Tetra New Material Technology Co., Ltd), 1-methylimidazole (99.0%, Aladdin), hydrogen peroxide (H_2O_2, 30%, SCR), formic acid (HCOOH, 98%, SCR), and divinylbenzene (DVB, 80% of *ortho*-, *meta*-, and *para*-isomers, Aladdin) were used as received. Methylhexahydrophthalic anhydride was kindly provided by Shanghai Kangda Chemical New Material Group Co., Ltd. Spherical silica nano-objects (SiO_2-1#, SiO_2 > 95% and SiO_2-2#, SiO_2 > 95%) were kindly provided by Denka. All other reagents were purchased from SCR and used as received unless declared otherwise.

Preparation of stabilized nano-objects *via* the LAPISA process

According to our previous works,[48] the PDVB@(PI-*b*-PS) nano-objects were synthesized *via* a LAPISA process and *in situ* crosslinked with DVB monomers. Using the synthesis of the stabilized $PDVB_{25}$@(PI_{82}-*b*-PS_{105}) as an example, the detailed procedures were illustrated as follows. First, the dried Is (9.0 mL, 6.10 g), TMEDA (0.30 mL), and *n*-heptane (120 mL, 81.90 g) were sequentially added into a dried 250 mL round-bottom flask equipped with a stirrer, and the flask was charged with argon. Before the addition of the measured *n*-Bu$^-$Li$^+$ solution (0.60 mL, 0.96 mmol), the impurities in the flask were consumed *via* dropwise addition of *n*-Bu$^-$Li$^+$. After 2.0 h, 0.50 mL of the mixture was withdrawn for characterization. Subsequently, the St (13.5 mL, 12.10 g) was added. After 4.0 h, 0.50 mL of the mixture was withdrawn for characterization. Finally, the DVB (4.50 mL, 4.10 g) was added and the polymerization was terminated with 0.20 mL methanol after another 18.0 h. The nano-objects were purified and recovered *via* precipitation from methanol three times. PI_{82} macroinitiator, SEC: $M_{n,SEC}$ = 5600 g mol^{-1}, M_w/M_n = 1.09. PI_{82}-*b*-PS_{105} diblock copolymer, SEC: $M_{n,SEC}$ = 16 500 g mol^{-1}, M_w/M_n = 1.06. $PDVB_{25}$@(PI_{82}-*b*-PS_{105}), ^{1}H NMR ($CDCl_3$, δ, ppm, TMS): 0.82 (C***H***$_3$CH$_2$– on residual *n*-butyl group), 1.23–2.26 (m, –C(C***H***$_3$)– on PI, aliphatic main chain-C***H***$_2$C***H***– on PS), 4.60–4.70 (–(CH$_3$)C=C***H***$_2$ of 3,4-addition Is unit), 4.96 (–CH=C***H***$_2$ of 1,2-addition Is unit), 5.07 (–C***H***=C(CH$_3$)– of 1,4-addition Is unit), 5.71 (–C***H***=CH$_2$ of 1,2-addition Is unit), 6.29–7.30 (m, aromatic C$_6$***H***$_5$ on PS).

Similarly, the stabilized $PDVB_{60}$@(PI_{86}-*b*-PS_{228}), $PDVB_{82}$@(PI_{252}-*b*-PS_{313}), $PDVB_{129}$@PI_{239}, P(S_{317}-*co*-DVB_{90})@PI_{243}, $PDVB_{25}$@(PI_{76}-*b*-PS_{103}), and $PDVB_{73}$@(PI_{202}-*b*-PS_{278}) nano-objects were synthesized *via* the LAPISA process.

Preparation of stabilized nano-objects *via* the LAPICA process

According to our previous works,[49] the PDVB@(PI-*b*-PS/PS) nano-objects were synthesized *via* a LAPICA process and *in situ* crosslinked with DVB monomers. Using the synthesis of the stabilized $PDVB_{26}$@(PI_{85}-*b*-PS_{75}/PS_{38}) as an example, the detailed procedures were illustrated as follows. First, the dried Is (9.0 mL, 6.10 g), TMEDA (0.30 mL), and *n*-heptane (120 mL, 81.90 g) were sequentially added into a dried 250 mL round-bottom flask equipped with a stirrer, and the flask was charged with argon. Before the addition of the measured *n*-Bu$^-$Li$^+$ solution (0.60 mL, 0.96 mmol), the impurities in flask were consumed *via* dropwise addition of *n*-Bu$^-$Li$^+$. After 2.0 h, 0.50 mL of the mixture was withdrawn for characterization. Subsequently, the *n*-Bu$^-$Li$^+$ solution (1.20 mL, 1.92 mmol) and the St (13.5 mL, 12.10 g) were sequentially added. After 4.0 h, 0.50 mL of the mixture was withdrawn for characterization. Finally, the DVB (4.50 mL, 4.10 g) was added and the polymerization was terminated with 0.20 mL methanol after another 16.0 h. The nano-objects were purified and recovered *via* precipitation from methanol three times. PI_{85} macroinitiator, SEC: $M_{n,SEC}$ = 5800 g mol^{-1}, M_w/M_n = 1.09. PI_{85}-*b*-PS_{75} diblock copolymer, SEC: $M_{n,SEC}$ = 13 600 g mol^{-1}, M_w/M_n = 1.06. PS_{38} homopolymer, $M_{n,SEC}$ = 3900 g mol^{-1}, M_w/M_n = 1.06. $PDVB_{26}$@(PI_{85}-*b*-PS_{75}/PS_{38}), ^{1}H NMR ($CDCl_3$, δ, ppm, TMS): 0.82 (C***H***$_3$CH$_2$– on residual *n*-butyl group), 1.23–2.26 (m, –C(C***H***$_3$)– on PI, aliphatic main chain-C***H***$_2$C***H***– on PS), 4.60–4.70 (–(CH$_3$)C=C***H***$_2$ of 3,4-addition Is unit), 4.96 (–CH=C***H***$_2$ of 1,2-addition Is unit), 5.07 (–C***H***=C(CH$_3$)– of 1,4-addition Is unit), 5.71 (–C***H***=CH$_2$ of 1,2-addition Is unit), 6.29–7.30 (m, aromatic C$_6$***H***$_5$ on PS).

Similarly, the stabilized $PDVB_{84}$@(PI_{228}-*b*-PS_{203}/PS_{169}) nano-objects were synthesized *via* the LAPICA process.

Preparation of hydroxylated nano-objects *via* the thiol–ene reaction

The PI block on the nano-objects could be functionalized with 3-mercaptopropane-1,2-diol *via* the thiol–ene reaction, and hydroxyl groups were introduced. Using the modification of $PDVB_{25}$@(PI_{82}-*b*-PS_{105}) nano-objects as an example, the detailed procedure is illustrated as follows. First, the $PDVB_{25}$@(PI_{82}-*b*-PS_{105}) nano-objects (3.0 g) were added into a 250 mL round-bottom flask and dispersed in a mixture of THF (65 mL) and toluene (65 mL). Subsequently, 3-mercaptopropane-1,2-diol (0.25 g, 2.30 mmol) and AIBN (100.0 mg, 0.63 mmol) were sequentially added. After the oxygen in the flask was replaced by bubbling with argon, the flask was placed in an oil bath at 65 °C for 24 h. The product was obtained *via* precipitation into methanol three times. The hydroxylated PI was labelled as HPI, and the nano-objects were labelled as $PDVB_{25}$@(HPI_{82}-*b*-PS_{105}). $PDVB_{25}$@(HPI_{82}-*b*-PS_{105}), ^{1}H NMR ($CDCl_3$, δ, ppm, TMS): 0.82 (C***H***$_3$CH$_2$– on residual *n*-butyl group), 1.23–2.26 (m, –C(C***H***$_3$)– on HPI, aliphatic main chain-C***H***$_2$C***H***– on PS, –SCH$_2$C***H***$_2$– on HPI), 2.37–2.77 (m, –C***H***$_2$SC***H***$_2$–), 3.47–3.88 (m, HOC***H***$_2$C***H***(OH)–), 4.60–4.70 (–(CH$_3$)C=C***H***$_2$ of 3,4-addition Is unit), 4.96 (–CH=C***H***$_2$ of 1,2-addition Is unit), 5.07 (–C***H***=C

(CH_3)– of 1,4-addition Is unit), 6.29–7.30 (m, aromatic –$C_6\boldsymbol{H}_5$ on PS).

Preparation of epoxidized nano-objects *via* the epoxidation reaction

The 1,4-addition Is units on the nano-objects could be epoxidized in the presence of H_2O_2/HCOOH agents. Using the epoxidation of $PDVB_{25}$@(PI_{76}-*b*-PS_{103}) nano-objects as an example, the detailed procedures were illustrated as follows. The $PDVB_{25}$@(PI_{76}-*b*-PS_{103}) nano-objects (3.0 g) were firstly dispersed into toluene (100.0 mL) in a 250 mL round-bottom flask. Subsequently, the HCOOH (0.72 mL) and H_2O_2 (4.42 mL) were sequentially added. After the flask was placed into an oil bath at 50 °C for 2.0 h, the product was obtained *via* precipitation into methanol three times. The epoxidized PI was labelled as EPI, and the nano-objects were labelled as $PDVB_{25}$@(EPI_{76}-*b*-PS_{103}). $PDVB_{25}$@(EPI_{76}-*b*-PS_{103}), ^{1}H NMR ($CDCl_3$, δ, ppm, TMS): 0.82 ($C\boldsymbol{H}_3CH_2$– on residual *n*-butyl group), 1.23–2.26 (m, –C($C\boldsymbol{H}_3$)– on EPI, aliphatic main chain-$C\boldsymbol{H}_2C\boldsymbol{H}$– on PS), 2.60–2.85 (m, –COC$\boldsymbol{H}CH_2$–), 4.60–4.70 (–(CH_3)C═C$\boldsymbol{H}_2$ of 3,4-addition unit), 6.29–7.30 (m, aromatic $C_6\boldsymbol{H}_5$ on PS).

Epoxy resin modified with hydroxylated or epoxidized nano-objects

Using the hydroxylated $PDVB_{25}$@(HPI_{82}-*b*-PS_{105}) nano-objects as an additive for epoxy resin, the detailed procedures were illustrated as follows. First, the epoxy resin UVR-6110 (2.10 g, 8.70 mmol), methylhexahydrophthalic anhydride (2.40 g, 14.30 mmol), and a dispersion of hydroxylated $PDVB_{25}$@(HPI_{82}-*b*-PS_{105}) nano-objects (0.10 g dried nano-objects in 2.30 mL THF) were sequentially added and mixed in a 100 mL round-bottom flask. After the THF solvent was completely evaporated out under vacuum, the catalyst 1-methylimidazole (16.0 mg, 0.20 mmol) was added. Finally, the mixture was cured on a hot plate at 125 °C for 30 min and further cured at 150 °C for 90 min, and the epoxy resin composite was thus prepared. The epoxy resin composite was labelled as $PDVB_{25}$@(HPI_{82}-*b*-PS_{105})@Epoxy.

Similarly, the epoxy resins modified with epoxidized nano-objects, SiO_2-1# or SiO_2-2# were prepared using a similar procedure. By varying the weight ratio of nano-objects to UVR-6110, the contents of the nano-objects were modulated as 4.5 wt%, 9.0 wt% and 15.0 wt%, respectively.

Instruments and characterization

The molecular weight (MW) and molecular weight distribution (M_w/M_n) of the polymers were analysed *via* size exclusion chromatography (SEC) measurements, which were performed in THF at 35 °C with an elution rate of 1.0 mL min^{-1} on an Agilent 1100 equipped with a G1310A pump, a G1362A refractive index detector, and a G1314A variable wavelength detector. One 5 μm LP gel column (molecular weight range 500–2 × 10^4 g mol^{-1}) and two 5 μm LP gel mixed bed columns (molecular weight range 200–3 × 10^6 g mol^{-1}) were calibrated using PS standards. The injection volume was 20 μL, and the concentration was 5–10 mg mL^{-1}. The proton nuclear magnetic resonance (^{1}H NMR) spectra of the polymers were recorded on a Bruker (400 MHz) spectrometer in $CDCl_3$ with tetramethylsilane (TMS) as the internal reference at 298 K. Dynamic light scattering (DLS) using a Malvern Zetasizer Nano ZS90 was employed to determine the average hydrodynamic diameters and distributions, and the scattered light was detected at an angle of 173°. The differential scanning calorimetry (DSC) measurements were performed using a TA DSC250 instrument under a nitrogen flow rate of 50 mL min^{-1}. For the diblock copolymer or nano-objects, the samples were first heated from −65 °C to 150 °C at a heating rate of 10 °C min^{-1} under a nitrogen atmosphere (1st run), followed by cooling to −65 °C at −10 °C min^{-1} after stopping at 150 °C for 1 minute (2nd run), then from −65 °C to 150 °C at a heating rate of 10 °C min^{-1} after stopping at −65 °C for 1 minute (3rd run). For the composites, a similar procedure was adopted, except that the temperature range was set between 25 °C and 250 °C. Thermogravimetric analysis (TGA) was performed on a Mettler instrument. The samples were heated from 50 to 600 °C with a heating ramp of 10 °C min^{-1} in an atmosphere of nitrogen. The thermal expansion behaviours of the samples were measured using a Mettler Toledo-SDTA841e thermomechanical analyser (TMA), with measurements performed from 30 °C to 240 °C at a heating rate of 10 °C min^{-1} under a nitrogen flow rate of 50 mL min^{-1}. Transmission electron microscopy (TEM) was performed using a HITACHI-HT7800 Plus microscope operated at 120 kV. The as-prepared nano-objects were diluted in THF to give 0.02 wt%–0.06 wt% dispersions. After one drop of the dispersion was deposited onto carbon-coated copper grids, the copper grids were dried in air for 24 h and used for TEM measurements. Ultrathin sections of the cured epoxy resin composites were cut using a Leica cryo-ultramicrotome (FC7-UC7) and used for TEM measurements.

Conclusions

In summary, stabilized spherical and worm-like organic nano-objects with different sizes and morphologies were prepared *via* a LAPISA or LAPICA process in a one-pot manner. After thiol–ene or epoxidation reactions on the double bonds of the PI block, hydroxyl and epoxy groups were introduced onto the nano-objects. The miscibility or compatibility of the nano-objects with epoxy resin was greatly improved and the functionalized nano-objects were smoothly introduced into epoxy resin. The DSC, TGA and TMA analyses affirmed that the organic nano-objects could improve the thermal properties of epoxy resin composites, which were obviously superior to the composites with the diblock copolymer or inorganic silica nano-objects. Generally, the composites with smaller spherical nano-objects had higher T_g than those with larger spherical ones or worm-like ones, which showed that the sizes and morphologies exhibited significant effects on the T_gs. The TEM images showed that the organic nano-objects could be uniformly distributed into the epoxy resin and the interfaces were

actually integrated, which was attributed to the intrinsic reason for the improved T_gs of the composites. The results in this work provided an alternative route to modify epoxy resin composites, further enriching the applications of nano-objects in the PISA process.

Data availability

Further data could be supplied by the authors upon request.

Conflicts of interest

There are no conflicts to declare.

Acknowledgements

We appreciate the financial support of this research by the Natural Science Foundation of China (22271058).

References

1 O. Vryonis, T. Andritsch, A. S. Vaughan and P. L. Lewin, *IEEE Conf. Electr. Insul. Dielectr. Phenom.*, 2016, 635–638.
2 K. Moyer, C. Z. Meng, B. Marshall, O. Assal, J. Eaves, D. Perez, R. Karkkainen, L. Roberson and C. L. Pint, *Energy Storage Mater.*, 2020, **24**, 676–681.
3 B. K. Muñoz, A. del Bosque, M. Sánchez, V. Utrilla, S. G. Prolongo, M. G. Prolongo and A. Ureña, *Polymer*, 2021, **214**, 123233.
4 F. Djouani, C. Connan, M. M. Chehimi and K. Benzarti, *Surf. Interface Anal.*, 2008, **40**, 146–150.
5 Y. F. Wen, C. Chen, Y. S. Ye, Z. G. Xue, H. Y. Liu, X. P. Zhou, Y. Zhang, D. Q. Li, X. L. Xie and Y. W. Mai, *Adv. Mater.*, 2022, **34**, 2201023.
6 D. R. Xin and Q. Han, *J. Mol. Model.*, 2015, **21**, 5.
7 H. Ghazali, L. Ye and A. N. Amir, *Polym. Polym. Compos.*, 2021, **29**, S1317–S1327.
8 F. L. Jin, X. Li and S. J. Park, *J. Ind. Eng. Chem.*, 2015, **29**, 1–11.
9 Y. Ge, X. Q. Zhang, Y. Shi, Y. B. Cai, S. T. Zhou, M. Liang and H. W. Zou, *Mater. Chem. Front.*, 2021, **5**, 8387–8396.
10 Q. Wu, Q. Q. Wan, X. Yang, F. Wang and J. F. Zhu, *Appl. Surf. Sci.*, 2021, **547**, 149162.
11 S. Warwel and F. Brüse, *J. Surfactants Deterg.*, 2004, **7**, 187–193.
12 P. Mohan, *Polym.-Plast. Technol. Eng.*, 2013, **52**, 107–125.
13 R. Bagheri, B. T. Marouf and R. A. Pearson, *Polym. Rev.*, 2009, **49**, 201–225.
14 F. Liu, Z. Q. Wang, W. Y. Liang and Y. W. Qu, *Adv. Mater. Res.*, 2012, **383–390**, 3845–3848.
15 M. Ukaji, M. Takamura, K. Shirai, W. Gang, T. Yamauchi and N. Tsubokawa, *Polym. J.*, 2008, **40**, 607–613.
16 N. K. Naik, K. S. Pandya, V. R. Kavala, W. Zhang and N. A. Koratkar, *Polym. Eng. Sci.*, 2014, **54**, 2896–2901.
17 M. Aliakbari, O. M. Jazani, M. Sohrabian, M. Jouyandeh and M. R. Saeb, *Prog. Org. Coat.*, 2019, **133**, 376–386.
18 M. P. Jenarthanan, K. Marappan and R. Giridharan, *Pigm. Resin Technol.*, 2019, **48**, 243–248.
19 M. Megahed, S. M. Youssef, S. S. Ali-Eldin and M. A. Agwa, *Fibers Polym.*, 2021, **22**, 1063–1081.
20 J. Datta and M. Wloch, *Polym. Bull.*, 2014, **71**, 3035–3049.
21 L. Liu, Y. D. Huang, Z. Q. Zhang and X. B. Yang, *J. Appl. Polym. Sci.*, 2006, **99**, 3172–3177.
22 Y. J. Liu, J. Y. Lu and Y. B. Cui, *Carbon Resour. Convers.*, 2020, **3**, 29–35.
23 M. Dong, H. Zhang, L. Tzounis, G. Santagiuliana, E. Bilotti and D. G. Papageorgiou, *Carbon*, 2021, **185**, 57–81.
24 M. Wloch, F. Baginski, P. Kozinski and J. Datta, *Polym. Polym. Compos.*, 2020, **28**, 484–491.
25 C. Gao, Z. H. Zhu, Y. C. Shen, T. W. Wang and D. Xiang, *Composites, Part B*, 2020, **198**, 108232.
26 X. Y. Lv, Y. Sun, Z. C. Jiang, Y. H. Zhang and M. W. Di, *Adv. Mater. Sci. Technol.*, 2011, **181–182**, 99–102.
27 F. C. Lü, J. X. Song, H. O. Ruan, M. Y. Zhu, S. S. Wang, P. Lü and Q. Xie, *Polym. Compos.*, 2022, **43**, 347–357.
28 A. M. Atta, A. F. El-Kafrawy, M. H. Aly and A.-A. A. Abdel-Azim, *Prog. Org. Coat.*, 2007, **58**, 13–22.
29 K. Song, Y.-T. Pan, J. Zhang, P. Song, J. He, D.-Y. Wang and R. Yang, *Chem. Eng. J.*, 2023, **468**, 143653.
30 S. Waskiewicz, K. Zenkner, E. Langer, M. Lenartowicz and I. Gajlewicz, *Prog. Org. Coat.*, 2013, **76**, 1040–1045.
31 B.-y. Shi and G.-w. Wang, *Acta Polym. Sin.*, 2022, **53**, 15–29.
32 B. Charleux, G. Delaittre, J. Rieger and F. D'Agosto, *Macromolecules*, 2012, **45**, 6753–6765.
33 G. Wang, M. Schmitt, Z. Y. Wang, B. Lee, X. C. Pan, L. Y. Fu, J. J. Yan, S. P. Li, G. J. Xie, M. R. Bockstaller and K. Matyjaszewski, *Macromolecules*, 2016, **49**, 8605–8615.
34 D. J. Rucco, B. E. Barnes, J. B. Garrison, B. S. Sumerlin and D. A. Savin, *Biomacromolecules*, 2020, **21**, 5077–5085.
35 A. Shahrokhinia, S. Rijal, B. S. Baghirzade, R. A. Scanga, P. Biswas, S. Tafazoli, O. G. Apul and J. F. Reuther, *Macromolecules*, 2022, **55**, 3699–3710.
36 A. Darabi, P. G. Jessop and M. F. Cunningham, *Macromolecules*, 2015, **48**, 1952–1958.
37 X. G. Qiao, O. Lambert, J. C. Taveau, P. Y. Dugas, B. Charleux, M. Lansalot and E. Bourgeat-Lami, *Macromolecules*, 2017, **50**, 3796–3806.
38 X. G. Qiao, P. Y. Dugas, B. Charieux, M. Lansalot and E. Bourgeat-Lami, *Macromolecules*, 2015, **48**, 545–556.
39 M. Lages, N. Gil, P. Galanopoulo, J. Mougin, C. Lefay, Y. Guillaneuf, M. Lansalot, F. D'Agosto and J. Nicolas, *Macromolecules*, 2022, **55**, 9790–9801.
40 S. Q. Yang, L. Zhang, Y. Chen and J. B. Tan, *Macromolecules*, 2022, **55**, 8472–8484.
41 X. Wang, S. K. Man, J. W. Zheng and Z. S. An, *ACS Macro Lett.*, 2018, **7**, 1461–1467.
42 N. J. Warren, O. O. Mykhaylyk, D. Mahmood, A. J. Ryan and S. P. Armes, *J. Am. Chem. Soc.*, 2014, **136**, 1023–1033.

43 S. E. Woods, J. D. Tinkler, N. Bensabeh, M. Palà, S. J. Martin, I. Martin-Fabiani, G. Lligadas and F. L. Hatton, *ACS Sustainable Chem. Eng.*, 2023, **11**, 9979–9988.
44 N. Zaquen, H. J. Zu, A. M. N. B. P. H. A. Kadir, T. Junkers, P. B. Zetterlund and C. Boyer, *ACS Appl. Polym. Mater.*, 2019, **1**, 1251–1256.
45 D. B. Wright, M. A. Touve, L. Adamiak and N. C. Gianneschi, *ACS Macro Lett.*, 2017, **6**, 925–929.
46 D. Shen, B. Y. Shi, P. Zhou, D. Li and G. W. Wang, *Macromolecules*, 2023, **56**, 4814–4822.
47 P. J. Hurst, A. A. Graham and J. P. Patterson, *ACS Polym. Au*, 2022, **2**, 501–509.
48 J. Wang, M. Y. Cao, P. Zhou and G. W. Wang, *Macromolecules*, 2020, **53**, 3157–3165.
49 J. W. Zhang, P. Zhou, B. Y. Shi, P. H. Li and G. W. Wang, *Macromolecules*, 2023, **56**, 5743–5753.
50 C. Zhu and J. Nicolas, *Biomacromolecules*, 2022, **23**, 3043–3080.
51 C. E. Ellis, J. D. Garcia-Hernandez and I. Manners, *J. Am. Chem. Soc.*, 2022, **144**(44), 20525–20538.
52 K. Li, P. Y. Dugas, E. Bourgeat-Lami and M. Lansalot, *Polymer*, 2016, **106**, 249–260.
53 W. Zhou, Q. W. Qu, W. J. Yu and Z. S. An, *ACS Macro Lett.*, 2014, **3**, 1220–1224.
54 J. Demarteau, A. F. de Añastro, A. S. S. Shaplov and D. Mecerreyes, *Polym. Chem.*, 2020, **11**, 1481–1488.
55 R. Albiges, P. Klein, S. Roi, F. Stoffelbach, C. Creton, L. Bouteiller and J. Rieger, *Polym. Chem.*, 2017, **8**, 4992–4995.
56 R. Jérôme and J. D. Tong, *Curr. Opin. Solid State Mater. Sci.*, 1998, **3**, 573–578.
57 A. Hirao, R. Goseki and T. Ishizone, *Macromolecules*, 2014, **47**, 1883–1905.
58 S. P. Armes, S. Perrier and P. B. Zetterlund, *Polym. Chem.*, 2021, **12**, 8–11.
59 S. L. Canning, G. N. Smith and S. P. Armes, *Macromolecules*, 2016, **49**, 1985–2001.
60 F. D'Agosto, J. Rieger and M. Lansalot, *Angew. Chem., Int. Ed.*, 2020, **59**, 8368–8392.
61 T. Tang, J. Huang, B. Huang, J. Huang and G. Wang, *J. Polym. Sci., Part A: Polym. Chem.*, 2012, **50**, 5144–5150.
62 G. Wang, X. Fan and J. Huang, *J. Polym. Sci., Part A: Polym. Chem.*, 2010, **48**, 3797–3806.
63 A. Challioui, D. Derouet, A. Oulmidi and J. C. Brosse, *Polym. Int.*, 2004, **53**, 1052–1059.
64 R. B. Grubbs, M. E. Broz, J. M. Dean and F. S. Bates, *Macromolecules*, 2000, **33**, 2308–2310.